Pergamon

Int. J. Heat Mass Transfer. Vol. 41, No. 10, pp. 1267–1277, 1998

Printed in Great Britain
0017-9310/98 $19.00+0.00

PII: S0017-9310(97)00245-7

Augmentation of convective heat transfer by a torsionally-oscillating endwall disk

TAE GYU LIM and JAE MIN HYUN*

Department of Mechanical Engineering, Korea Advanced Institute of Science and Technology, 373-1 Kusong-dong Yusong-gu, Taejon 305-701, South Korea

(*Received* 1 *April* 1997 *and in final form* 13 *June* 1997)

Abstract—An investigation is made of fluid flow and heat transfer characteristics in a vertically-mounted circular cylinder. Motions are generated by the top endwall disk, which oscillates about the central axis with rotation rate $\Omega = \varepsilon\lambda\cos(\lambda t)$. The temperature of the top disk is higher than that of the bottom disk, producing a stable stratification of Brunt–Vaisala frequency N. Numerical solutions are acquired to the time-dependent Navier–Stokes equations. Comprehensive velocity and temperature data are obtained, which illustrate salient features of quasi-steady periodic flows. As the stratification increases, the steady meridional streaming is confined to a narrow region close to the top disk. Resonance is identified at particular values of (N/λ), when the system is excited at correct natural frequencies. An elementary inviscid analysis indicates the modes of inertial–gravity oscillations, and the present numerical data are in close agreement with the inviscid results. The amplitudes of fluctuating parts of meridional flow and of Nusselt number display distinctive peaks under resonance conditions. Details of evolutions of fluctuating velocities and temperatures are scrutinized to offer physical explanations for resonance. © 1998 Elsevier Science Ltd.

1. INTRODUCTION

Flow driven by a rotating disk has posed a long-standing fundamental problem. An elementary classical model was conceived by von Karman, which dealt with an infinite disk rotating steadily in an infinite expanse of a homogeneous viscous fluid. Similarity solutions were obtained for the three-component axisymmetric velocity field (see, e.g., Schlichting, 1968). Flows maintained by a steadily-rotating finite endwall disk lid in a closed circular cylinder, for large rotational Reynolds numbers, have been investigated extensively. These constitute crucial issues in both the basic fluid dynamics research and a multitude of technological applications (e.g., Pao, 1971; Alonso, 1975; Bertela and Gori, 1982; Lang *et al.*, 1994; Lim and Hyun, 1997).

The majority of preceding studies were concerned with the cases when the rotation rate of the disk is constant. Time-dependent flows, which arise when the rotation rate of the disk is time-variant, have not received much attention in the literature. The practical relevance of a temporally-varying rotation of disk can easily be appreciated by noting that the output from the electric motor drive in the laboratory turntable is seldom steady and constant. A canonical flow model can be constructed when the rotation rate of the disk is oscillatory in time. Early theoretical studies of flow induced by torsional oscillations of a disk were reported by Rosenblat (1959) and Benney (1964). These investigations assumed a small-amplitude torsional oscillation of an infinite plane disk in an unbounded constant-density fluid. By means of a linearized analysis, these works provided qualitative descriptions of the primary flow and identified a second-order meridional flow. In particular, the structure of steady and fluctuating parts of meridional flow was depicted. Lim and Hyun (1997) acquired numerical solutions to the full Navier–Stokes equations for an oscillating disk in a closed cylinder. The azimuthal and meridional flows when the amplitude of oscillation is finite were examined, and the qualitative patterns of meridional steady streaming were verified by laboratory flow visualizations. These reports supplied baseline information on the axisymmetric flows at large rotational Reynolds numbers when the disk undergoes torsional oscillations.

Analysis of heat (and/or mass) transfer from a rotating disk, in conjunction with the induced flow field, has been performed in several rudimentary configurations (Sparrow and Gregg, 1960; Kreith *et al.*, 1963; Lehmkuhl and Hudson, 1971). These earlier accounts were concerned with the changes in transport properties in the fluid due to the presence of one or more steadily-rotating disks. Experimental measurements of mass transfer from the steadily-rotating disks were obtained, and heat transfer coefficients were estimated by resorting to the analogy between heat and mass transfers.

The present paper explores the flow and heat trans-

* Author to whom correspondence should be addressed.

fer properties from a torsionally-oscillating disk in a vertically-mounted cylinder. Specifically, the oscillating disk, which constitutes the top endwall, is held at a higher temperature than the stationary bottom endwall disk of the cylinder. In essence, the introduction of a vertical temperature contrast ΔT gives rise to a stable stratification, and the strength of stratification is characterized by the system Brunt–Vaisala frequency N. The case of a homogeneous constant-density fluid corresponds to $N = 0$ (or $\Delta T = 0$).

It is proposed here to portray the structures of velocity and temperature fields in the cylinder, both instantaneous and time-averaged. One overriding concern is to describe the augmentations in heat transfer induced by the oscillation of the top endwall disk. Obviously, in the absence of this endwall motion, no fluid flows are generated and the heat transfer will be purely conductive; and the Nusselt number at the endwall disk would be unity. The enhancement of heat transfer, owing to the convective activities in the fluid caused by the top endwall disk, is of primary interest. The present effort to probe into the heat transfer characteristics brings forth a more fundamental question on the existence of resonance in the stratified fluid system. Clearly, there are two major frequencies involved in the problem formulation; i.e., the Brunt–Vaisala frequency, which inherently represents the buoyancy effect in the system, and the frequency of oscillation of the disk, which reflects the externally-controllable system excitation frequency. A rudimentary reasoning points to the possibility of resonance if these two frequencies are related to each other. In a similar, but somewhat different context, the presence of resonance has been identified in the examples of mixed convection (Iwatsu *et al.*, 1992) and of natural convection with temporally-varying thermal boundary conditions (Lage and Bejan, 1993; Kwak and Hyun, 1996). The key contention is that, when the system natural frequency is related to the external forcing frequency, intensification of the amplitudes of time-dependent flow variables is realized. This phenomenon was termed resonance in the present context. Scaling arguments were put forth by Lage and Bejan (1993) to estimate the resonance frequency for the case of a confined natural convection in a square cavity with temporally-oscillating heat fluxes at the sidewall. Numerical results were examined by Kwak and Hyun (1996) to derive the resonance frequency for a confined natural convection in a cavity with an oscillating sidewall temperature. The present endeavour aims to shed further light on the resonance in the case of a mixed convection in a cylinder in which forced convection is provided by the torsional oscillation of the top endwall disk.

Comprehensive numerical solutions to the governing time-dependent Navier–Stokes equations are produced. The wealth of numerical results allows a systematic evaluation of flow intensification and attendant heat transfer augmentations as the amplitude and frequency of the disk oscillation encompass broad ranges. The effects of the overall system rotational Reynolds number and of the strength of imposed vertical temperature difference ΔT are delineated. Emphasis will be placed on gaining an improved physical understanding of the nature of resonance pertinent to the present mixed convection problem formulation.

2. THE MODEL

Consider a vertically-mounted closed circular cylindrical container (radius R and height H; aspect ratio $Ar = H/R$), which is completely filled with an incompressible fluid of viscosity coefficient μ, specific heat C_p, and thermal conductivity k. The Boussinesq-fluid approximation is invoked, i.e., $\rho = \rho_B(1-\alpha(T-T_B))$, where ρ_B and T_B refer to the reference density and temperature at the bottom endwall disk ($z = 0$), respectively, and α the coefficient of thermometric volume expansion. These physical properties of the fluid are taken to be constant. The top endwall disk ($z = H$) executes a torsional oscillation with angular velocity $\Omega = \varepsilon\lambda\cos(\lambda t)$, and the rest of the solid walls of the cylinder are stationary. In the above expression, the frequency of torsional oscillation is λ and the dimensionless amplitude of the angular velocity is explicitly denoted by ε. Here, λ and ε should be treated as independent parameters, rather than forming a single parameter ($\varepsilon\lambda$) (see Rosenblat, 1959; Benney, 1964). The temperatures of the top disk ($z = H$) and bottom disk ($z = 0$) are, respectively, T_T and T_B, and, to insure a gravitationally stable temperature contrast, $\Delta T(= T_T - T_B) > 0$. The cylindrical sidewall is assumed to be thermally insulated (see Fig. 1).

It is advantageous here to implement non-dimensionalizations in the following fashion:

$$(r', z') = (r, z)/R;\quad t' = \lambda t;\quad (u', v', w') = (u, v, w)/(\lambda R);$$

$$p' = \frac{P}{\rho_B \lambda^2 R^2};\quad \theta = \frac{T - T_B}{\Delta T};$$

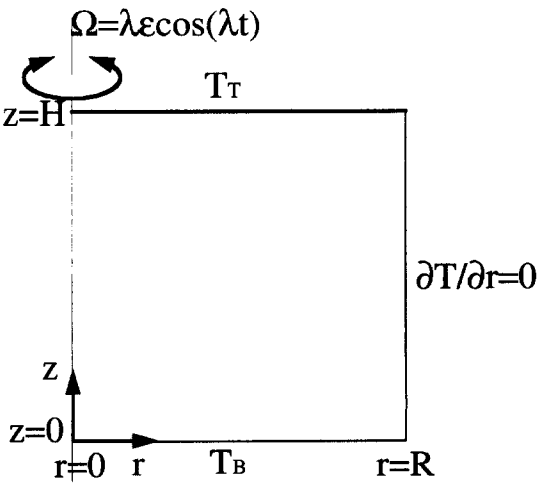

Fig. 1. Flow configuration.

$$N=\left(\frac{\alpha g\Delta T}{H}\right)^{1/2};\quad St_\lambda=\left(\frac{H}{R}\right)^{1/2}\left(\frac{N}{\lambda}\right);\quad St=\frac{N}{\varepsilon\lambda}=\frac{St_\lambda}{\varepsilon};$$

$$Re_\lambda=\frac{\lambda R^2}{\mu/\rho_B};\quad Re=\frac{\varepsilon\lambda R^2}{\mu/\rho_B}=\varepsilon\,Re_\lambda;\quad Pr=\frac{\mu/\rho_B}{k/(\rho_B c_p)}.$$

Note that the Rayleigh number Ra and the mixed-convection parameter Ra/Re^2 can be derived as

$$Ra=\frac{g\alpha\Delta TR^3}{(\mu/\rho_B)(\kappa/\rho_B c_p)};\quad \frac{Ra}{Re^2}=St^2\cdot Pr.$$

In the above, prime denotes the dimensionless quantities, and g the gravity. The principal nondimensional parameters are St_λ, the stratification number; Re, the rotational Reynolds number; and Pr, the Prandtl number: and ε denotes the dimensionless amplitude of torsional oscillation of the top endwall disk. Furthermore, it can be rewritten that $St_\lambda^2=Ra/(Re_\lambda^2\,Pr)$. Note that St_λ represents basically the ratio between the Brunt–Vaisala frequency pertinent to the system N and the forcing frequency of disk oscillation λ, and it is modified by the aspect ratio.

The fluid motion is governed by the time-dependent axisymmetric Navier–Stokes equations, which, written in cylindrical polar coordinates (r,φ,z) with corresponding velocity components (u,v,w), read, in nondimensional form (primes are dropped from the dimensionless quantities):

$$\frac{\partial u}{\partial t}=-\frac{1}{r}\frac{\partial}{\partial r}(ruu)-\frac{\partial}{\partial z}(uw)+\frac{v^2}{r}-\frac{\partial p}{\partial r}+\frac{1}{Re_\lambda}\left[\frac{\partial}{\partial r}\frac{1}{r}\frac{\partial}{\partial r}(ru)+\frac{\partial^2 u}{\partial z^2}\right] \quad (2)$$

$$\frac{\partial v}{\partial t}=-\frac{1}{r}\frac{\partial}{\partial r}(ruv)-\frac{\partial}{\partial z}(vw)-\frac{vu}{r}+\frac{1}{Re_\lambda}\left[\frac{\partial}{\partial r}\frac{1}{r}\frac{\partial}{\partial r}(rv)+\frac{\partial^2 v}{\partial z^2}\right] \quad (3)$$

$$\frac{\partial w}{\partial t}=-\frac{1}{r}\frac{\partial}{\partial r}(ruw)-\frac{\partial}{\partial z}(uw)-\frac{\partial p}{\partial z}+\frac{1}{Re_\lambda}\left[\frac{1}{r}\frac{\partial}{\partial r}\left(r\frac{\partial w}{\partial r}\right)+\frac{\partial^2 w}{\partial z^2}\right]+St_\lambda^2\theta \quad (4)$$

$$\frac{\partial\theta}{\partial t}=-\frac{1}{r}\frac{\partial}{\partial r}(ru\theta)-\frac{\partial}{\partial z}(w\theta)+\frac{1}{Re_\lambda\cdot Pr}\left(\frac{1}{r}\frac{\partial}{\partial r}\left(r\frac{\partial\theta}{\partial r}\right)+\frac{\partial^2\theta}{\partial z^2}\right) \quad (5)$$

$$\frac{1}{r}\frac{\partial}{\partial r}(ru)+\frac{\partial w}{\partial z}=0. \quad (6)$$

Note that the present formulation pertains to three-component, axisymmetric velocity fields (see, e.g., Rosenblat, 1959; Benney, 1964; Schlichting, 1968).

Computations commence from an initially motionless state with a vertically-linear temperature profile, i.e., $\theta=z/Ar$, which pertains to the conductive heat transfer mode. At time zero, the prescribed torsional oscillation is imposed on the top endwall disk. The main thrust of the problem lies in the large-time, quasi-steady periodic behaviour, and the initial transitory approach is not of much interest. In accordance with the problem statement, the boundary conditions are

$$u=v=w=0,\quad \frac{\partial\theta}{\partial r}=0\quad \text{at}\quad r=1 \quad (7)$$

$$u=v=w=0,\quad \theta=0\quad \text{at}\quad z=0 \quad (8)$$

$$u=w=0,\quad v=\varepsilon r\cos t,\quad \theta=1\quad \text{at}\ z=Ar. \quad (9)$$

To satisfy numerical stability requirements, the boundary conditions at the central axis are applied at a small, but finite, radius ($r=r_i$) (see Warn-Varnas *et al.*, 1978; Hyun *et al.*, 1982, 1983):

$$u=0,\quad \frac{\partial(v/r)}{\partial r}=0,\quad \frac{\partial w}{\partial r}=0,\quad \frac{\partial\theta}{\partial r}=0\quad \text{at}\quad r=r_i. \quad (10)$$

The above system of equations is solved by utilizing a well-established finite-difference numerical methodology. The numerical procedure adopted is essentially a mark-and-cell type, and it has been validated in a large number of simulations of rotating and stratified flows (e.g., Warn-Varnas *et al.*, 1978; Hyun *et al.*, 1982, 1983; Lim and Hyun, 1997). The specifics of the numerical schemes and algorithms have been amply documented, and they are not reproduced here. The time step Δt was taken to be sufficiently small to insure both numerical stability and resolution of the results. For most computations, after extensive test runs, the mesh network selected was typically (50×60) in the $(r$–$z)$ meridional plane, and Δt was chosen such that one oscillating cycle consisted of 4096 $(=2^{12})$ time steps. It was set $r_i=0.001$, and changes in r_i in the range $0.001\leqslant r_i\leqslant 0.005$ produced no noticeable alterations in the global flow patterns. Comprehensive convergence tests with respect to grid spacing and time interval were carried out, and the outcome was satisfactory (see the quantitative verifications in Lim and Hyun, 1997).

In order to deal with the upper corner region, two sets of grid-arrangement were extensively tested: (1) when the upper corner is part of the rotating disk and (2) when the upper corner belongs to the stationary sidewall. The global flow patterns obtained displayed virtually no differences between the above two cases when the present stretched grid network was deployed.

3. RESULTS AND DISCUSSION

In most runs, about five to ten oscillation cycles were needed to settle down to the quasi-steady state.

Also, it was set $Ar = 1.0$ and $Pr = 1.0$, and interest was focused on the explicit effects of the disk oscillations, which are characterized by ε and Re_λ, and of the influence of imposed vertical stratification, which is represented by St_λ. Also, for the present problem formulation, $St^2 = Ra/Re^2$.

It is useful to define the cycle-averaged value, denoted by subscript s, and the time-fluctuating component, shown by subscript f, i.e.,

$$\phi(t) = \phi_s + \phi_f(t)$$

where $\phi_s \equiv \int_t^{t+2\pi} \phi \, dt$, in which ϕ stands for an instantaneous physical variable. Also, $A(\phi_f)$ represents the amplitude of the fluctuating component ϕ_f.

First, the effect of the buoyancy is scrutinized. Figure 2 illustrates the global patterns of the steady meridional streaming (u_s, w_s). In the plots, the meridional stream function ψ_s, which is defined such that $u_s = (1/r)(\partial\psi/\partial z)$, $w_s = -(1/r)(\partial\psi/\partial r)$, is shown. The parameters are $\varepsilon = 2.0$, $Re = 1000$. As is apparent in Fig. 2, the oscillation of the top disk generates steady axial motions toward the top disk at small and moderate radii. In the vicinity of the oscillating disk, the fluid is propelled radially outward. At large radii near the cylindrical sidewall, constrained by the finite geometry, the meridional flow turns away from the oscillating disk and points downward along the vertical sidewall. This completes the overall circulatory path, and this general behaviour was corroborated by flow visualizations for a homogeneous fluid (Lim and Hyun, 1997). The impact of buoyancy reduces, in general, the magnitudes of the meridional velocities, as shown in Fig. 2 (note the difference in scales for the values of Ψ_s of Fig. 2). The introduction of stable stratification suppresses vertical motions, therefore, as St increases, the region of appreciable meridional flows tends to be confined to the area closer to the oscillating disk. As seen in Fig. 2(c), when St is large, the meridional flows in the bulk of the interior, with the exception of a small zone adjacent to the disk, are practically nil.

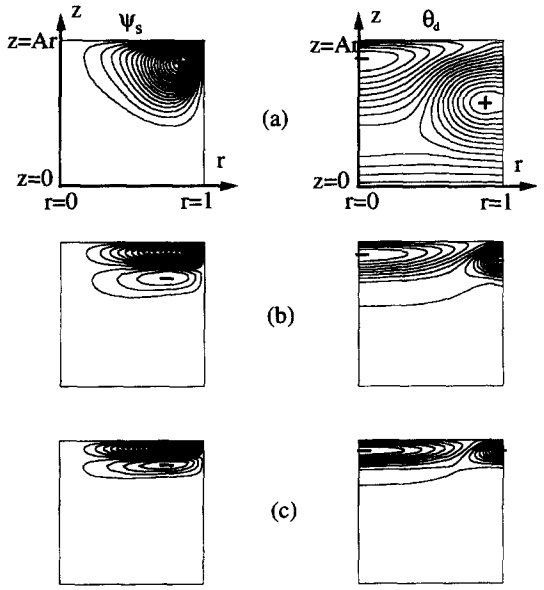

Fig. 2. Left column shows the stream function Ψ_s, for steady meridional flows (u_s, w_s), scaled by $Re_\lambda^{-1/2}$. Right column shows θ_d, the deviation of steady temperature (θ_s) from the original linear profile, i.e., $\theta_d \equiv \theta_s - z/Ar$. $\varepsilon = 2.0$, $Re = 1000$. (a) $St = 0.1$. $\Psi_{max} = 5.702 \times 10^{-3}$, $\Psi_{min} = -0.187 \times 10^{-3}$, $\Delta\psi = 2.94 \times 10^{-4}$, $\theta_{max} = 3.285 \times 10^{-1}$, $\theta_{min} = -1.334 \times 10^{-1}$, $\Delta\theta = 2.31 \times 10^{-2}$; (b) $St = 1.3$. $\Psi_{max} = 2.033 \times 10^{-3}$, $\Psi_{min} = -0.443 \times 10^{-3}$, $\Delta\Psi = 1.24 \times 10^{-4}$; $\theta_{max} = 0.665 \times 10^{-1}$, $\theta_{min} = -0.211 \times 10^{-1}$, $\Delta\theta = 0.438 \times 10^{-2}$; (c) $St = 5.0$. $\Psi_{max} = 0.724 \times 10^{-3}$, $\Psi_{min} = -0.211 \times 10^{-3}$, $\Delta\Psi = 0.468 \times 10^{-4}$; $\theta_{max} = 0.137 \times 10^{-1}$, $\theta_{min} = -0.0811 \times 10^{-1}$, $\Delta\theta = 0.109 \times 10^{-2}$.

The plots of the deviation of the time-averaged temperature θ_s from the initial-state vertically-linear profile z/Ar are also illustrated in Fig. 2, i.e., $\theta_d = \theta_s - z/Ar$. It is discernible that as stratification increases, the size of the area in which θ_d is appreciable shrinks, and this zone tends to be concentrated toward the oscillating top disk. Also, the magnitude of θ_d is reduced substantially as St increases. Under complete dominance of conduction, θ_d vanishes. Therefore, as seen in Fig. 2, the presence of non-vanishing θ_d points to convective activities. As the overall imposed stratification increases (see Fig. 2(c)), heat transport in much of the interior region, except in a narrow zone close to the top disk, is accomplished by conduction. As displayed earlier, the fluid is pumped from below toward the oscillating disk at small and moderate radii. Therefore, the fluid in the upper part of the cylinder is replaced by the colder fluid originating from the lower part of the cylinder. In the upper region of the cylinder of large radii near the vertical sidewall, the warm fluid near the top disk is propelled radially outward and it descends. These spatially-varying features of temperature fields are more conspicuous as St increases, and only in the upper part of the cylinder the averaged temperature field deviates from the initial linear temperature distribution. In the middle and bottom portions of the cylinder, the fluid temperature remains virtually unchanged from the conduction-controlled vertically linear profile. In the upper region of the cylinder, convection is dominant. Due to the disk oscillation, the fluid at small and moderate radii is colder than the initial state, and the fluid at large radii is warmer than the initial state. It is important to note that the oscillation of the upper disk brings forth radial temperature gradients in the regions of intense convective activities.

In the computation of N, the original linear temperature profile is used. In the presence of disk oscillation, the strictly-linear temperature profile cannot be maintained. However, as shown in Fig. 2, the deviations of temperature profile from the original linear profile are very small (note the order of magnitude of θ_d in Fig. 2). It then follows that, in the evaluation of stability, the use of the linear profile in N is justified.

As to the azimuthal flows, much of the descriptive statement of Lim and Hyun (1997) for the case of a homogeneous fluid is qualitatively applicable to the

present problem. The azimuthal velocity field is restricted to a region adjacent to the oscillating disk, and the (dimensional) vertical extent of this region is scaled by the thickness of the Stokes layer, $O(\nu/\lambda)^{1/2}$, where ν stands for the kinematic viscosity. Except in this zone, the azimuthal velocities in much of the cylinder interior are practically zero. This general property of the v-field remains largely unaltered as St increases in the range of the present computations.

One central issue in the discussion of temporally-periodic rotating flows of a stratified fluid is the presence of inertia-gravity wave oscillations. As the classical treatise (e.g., Greenspan, 1968) demonstrated, the restoring forces due to the rotational effect and the gravity give rise to internal oscillations. In the present context, the fluid system is excited by the externally-controllable mechanical oscillation of the upper disk. Therefore, a fundamental consideration leads to the possibility of resonance if the frequency of the disk oscillation and the frequency of the intrinsic internal gravity-inertial oscillation are related. Under resonance conditions, the fluid motions are intensified and the resultant convective heat transfer is enhanced. The notion of resonance in natural convection in a non-rotating confined space, with periodic thermal forcings, has been dealt with recently (e.g., Lage and Bejan, 1993; Antohe and Lage, 1994, 1996, 1997; Kwak and Hyun, 1996). In the case of rotating flows of a homogeneous fluid, resonance phenomenon in connection with the inertial oscillations has been addressed (e.g., Aldredge, 1976). Iwatsu *et al.* (1993) identified the resonance conditions by monitoring the augmentation in a square cavity with an oscillating flat lid under an imposed vertical temperature differential.

Consider axisymmetric flows in a cylindrical container, filled with an inviscid, incompressible fluid with a vertically-linear stratification. By assuming a wave-like solution, the eigenfrequency σ_{mn} of this fluid system can be found, by undergoing an elementary analysis (see, e.g., Greenspan, 1968):

$$\sigma_{mn} = N\left[1+\left(\frac{\xi_m^2}{n^2\pi^2}Ar^2\right)^{-1}\right]^{-1/2}$$

with the corresponding eigenfunction in the form of (in dimensional notation)

$$J_0\left(\xi_m\frac{r}{R}\right)\sin\left(n\pi\frac{z}{H}\right),$$

where J_0 denotes the zeroth-order Bessel function. In the above, m and n are the integer indices denoting the (m,n)th mode in the (radial and axial) directions, N the previously-defined Brunt–Vaisala frequency, ξ_m the mth positive root of the first-order Bessel function. Clearly, σ_{mn} indicates the frequency of modes of inertial–gravity oscillations which are inherent to the rotating and stratified fluid system under present consideration.

As remarked earlier, a key argument is the presence of resonance when the above-cited eigenmodes of the system are excited and amplified if the externally-applied excitation frequency λ matches the correct natural frequency. The impetus of the present study is to establish the resonance phenomenon and to portray the intensification of flow and augmentation of convective heat transport.

It is useful to define the radially-averaged instantaneous Nusselt number at height z:

$$Nu(t,z) = 2\int_0^1\left[-Pr\cdot Re\cdot w\cdot\theta+\frac{\partial\theta}{\partial z}\right]r\,\mathrm{d}r.$$

This can further be divided into the cycle-averaged value Nu_s and the time-fluctuating component $Nu_f(t,z)$, i.e.,

$$Nu_s = \int_t^{t+2\pi} Nu(t,z)\,\mathrm{d}t,$$

$$Nu_f(t,z) = Nu(t,z) - Nu_s.$$

Detection of resonance can be made by inspecting the characteristics of the fluctuating parts of flow variables. Figure 3 exhibits the behaviour of $A(\Psi_f)$ at selected locations vs St_λ. Obviously, the meridional flows are vigorous in the interior region of the cylinder (note the difference in scales for $A(\psi_f)$ in Figs 3(a)–(c)). Clearly, the dominant mode of inertial–gravity oscillations is the (1, 1) mode. This mode corresponds to a disturbance whose radial extent fills the entire cylinder radius ($m = 1$), and a half-wave of this mode fits the whole cylinder height ($n = 1$). The afore-stated inviscid analysis yields $\sigma_{11} \cong 0.773N$, the second mode $\sigma_{12} \cong 0.521N$, and the third mode $\sigma_{13} \cong 0.377N$, etc. Also, since the rotation rate of the top disk, $\Omega(t)$, is sinusoidal with frequency λ, the pertinent frequency for the absolute magnitude of the rotation rate, $|\Omega(t)|$, is 2λ. Notice that the temporal behaviour of meridional flows is in response to $|\Omega(t)|$. Therefore, the base-mode resonance is expected when $2\lambda_{re} = \sigma_{11}$, which points to $St_{re} = Ar^{1/2}(N/\lambda_{re}) = 2.59$. In Fig. 3, it is evident that the primary peak in $A(\Psi_f)$ is seen at $St_\lambda \cong 2.6$, which is in close agreement with the above reasoning based on inviscid analysis. The secondary and tertiary peaks in $A(\Psi_f)$ in Fig. 3 are found $St_\lambda \cong 3.8$ and $St_\lambda \cong 5.3$, respectively. These correspond to the second and third modes of excitation, i.e., when $2\lambda = \sigma_{12}$ and $2\lambda = \sigma_{13}$, respectively. The overall results in Fig. 3 are supportive of the concept of flow intensification under resonance conditions, and the numerical values derivable from the inviscid theory are shown to be reasonably accurate in assessing the resonance frequencies.

Figure 4 demonstrates the variations of the kinetic energy (KE) of meridional flows. Here, KE is defined as

$$KE = \int_0^{Ar}\int_0^1 (u^2+w^2)r\,\mathrm{d}r\,\mathrm{d}z.$$

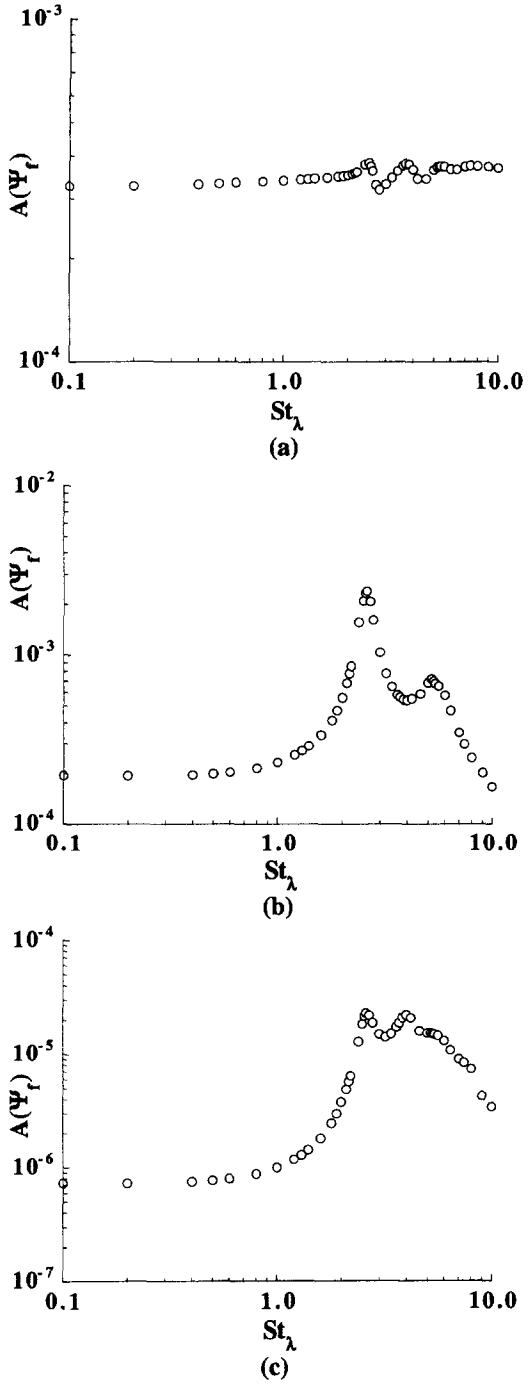

Fig. 3. Amplitude of the fluctuating part of meridional streaming, $A(\Psi_f)$, vs St_λ. $\varepsilon = 2.0$, $Re = 1000$. The radial location is $r = 0.5$, and vertical locations are: (a) $z/Ar = 0.98$; (b) $z/Ar = 0.5$; (c) $z/Ar = 0.02$.

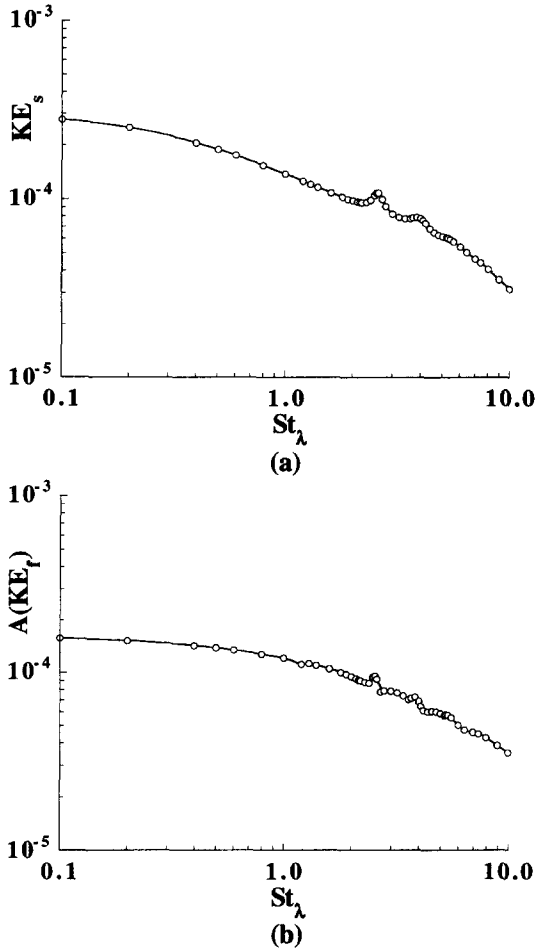

Fig. 4. Kinetic energies of meridional flow vs St_λ. (a) steady part; (b) fluctuating part. $\varepsilon = 2.0$, $Re = 1000$.

Obviously, the kinetic energy generally decreases with St_λ; as ascertained in Fig. 2, the overall meridional flows are attenuated as the system stratification is increased. In Fig. 4, the curves of kinetic energies display local peaks under resonance conditions, which is in line with the assertions of Fig. 3, i.e., $St_\lambda \cong 2.6$, 3.8, and 5.3 for local peaks. It is noted that the ordinates in Figs 3 and 4 are in logarithmic scales. These establish that the physical variables peak when the resonance conditions are met. For large values of Re and Ra, the inertial–gravity oscillations based on the inviscid consideration provide valid estimates of the eigenmodes of the system.

The enhancement of heat transport is illustrated in Figs 5 and 6. In Fig. 5, the explicit variation of $A(Nu_f)$ with St_λ is plotted. In the parameter values covered, the base-mode resonance condition, i.e., $St_\lambda \cong 2.6$, is largely unaffected as the amplitude of the disk oscillation ε varies. In the middle portion of the cylinder, the augmentation of the fluctuating part of heat transfer, $A(Nu_f)$, is most pronounced. The numerical results are reorganized in Fig. 6 to delineate the effect of St. The resonance points on the St_λ-axis remain virtually unchanged as the overall stratification increases, which is consistent with the foregoing physical arguments.

It is emphasized that the amplifications shown in Figs 5 and 6 refer to the amplitude of the fluctuating part of Nu. The changes in the time-averaged heat transport, expressed by Nu_s, are very small for the parameter ranges of present concern (Bejan and Lage,

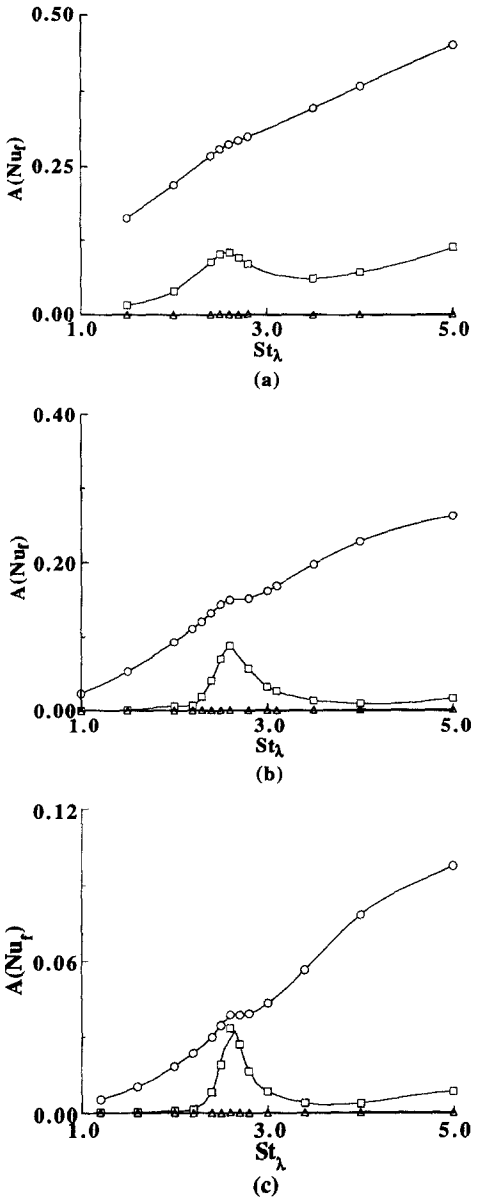

Fig. 5. Amplitude of fluctuating part of the Nusselt number, $A(Nu_f)$ vs St_λ. The vertical locations are: ○, $z/Ar = 0.98$; □, $z/Ar = 0.5$; △, $z/Ar = 0.02$. $Re = 1000$. Note that $St_\lambda = \varepsilon St$. (a) $St = 0.5$, (b) $St = 1.0$, (c) $St = 2.0$.

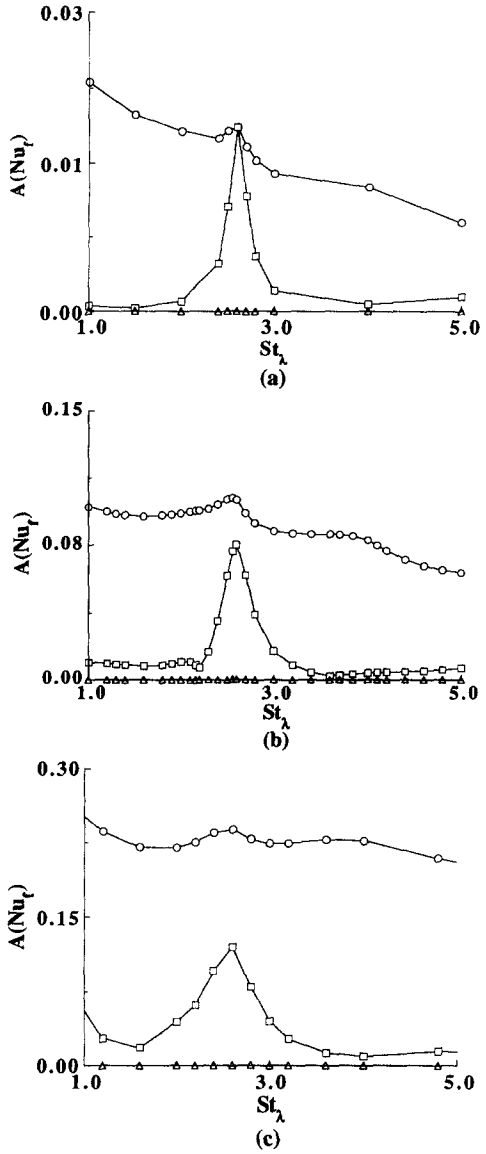

Fig. 6. Amplitude of fluctuating part of the Nusselt number, $A(Nu_f)$ vs St_λ. The vertical locations are: ○, $z/Ar = 0.98$; □, $z/Ar = 0.5$; △, $z/Ar = 0.02$. $Re = 1000$. (a) $\varepsilon = 1.0$, (b) $\varepsilon = 2.0$, (c) $\varepsilon = 4.0$.

1993; Antohe and Lage, 1994, 1996, 1997; Kwak and Hyun, 1996).

The general effect of Pr on resonance was discussed in detail in Antohe and Lage (1997) and Kwak and Hyun (1996). The overall resonance phenomenon is found to be most distinctive for $Pr \sim O(1)$, and the present study reports on the results for $Pr = 1.0$. The global qualitative observations are similar for other Pr values.

The details of the temporal variation of the Nu-profile are elaborated in Fig. 7. The intensification of Nu-profiles under resonance in the middle and bottom regions of the cylinder is in evidence (see Fig. 7(b)).

In plots displaying the instantaneous flow variables, the fluctuating parts are masked by the dominant steady features. However, in an effort to gain physical insight into the mechanism of resonance, it is useful to examine the details of the time-fluctuating components of flow. The ensuing discussions run closely to the physical pictures advanced by Kwak and Hyun (1996) for natural convection in a cavity with time-oscillating thermal boundary conditions.

The disk rotation can now be divided into four phases, as shown in Fig. 8. Phases I and III (II and IV) represent deceleration (acceleration) in the absolute magnitude of the rotation rate. It is important to note that the fluctuating part of meridional flow, relative to the steady motion, diminishes (intensifies) in phase I and III (II and IV). Here, it is stressed that the

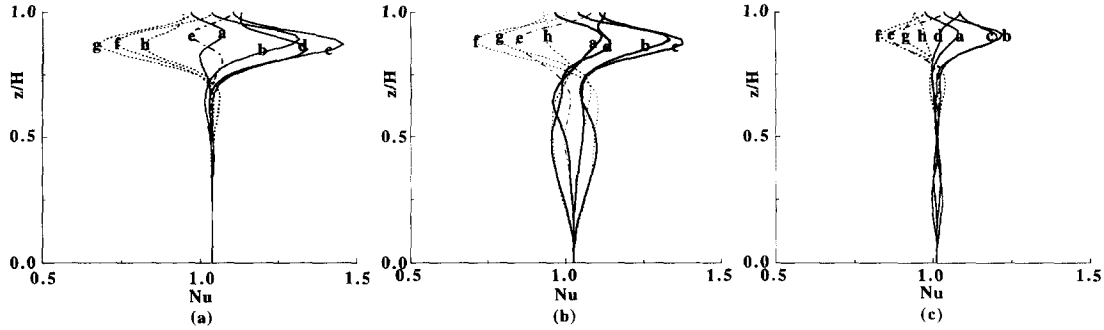

Fig. 7. Vertical profiles of the Nusselt number Nu, over a half cycle of the top disk oscillation. Conditions are $Re = 1000$, $\varepsilon = 2.0$. Times (λt) for the curves are: a, 0; b, $\pi/8$; c, $\pi/4$; d, $3\pi/8$; e, $\pi/2$; f, $5\pi/8$; g, $3\pi/4$; h, $7\pi/8$; i, π. (a) $St_\lambda = 2.0$, (b) $St_\lambda = 2.6$, (c) $St_\lambda = 3.0$.

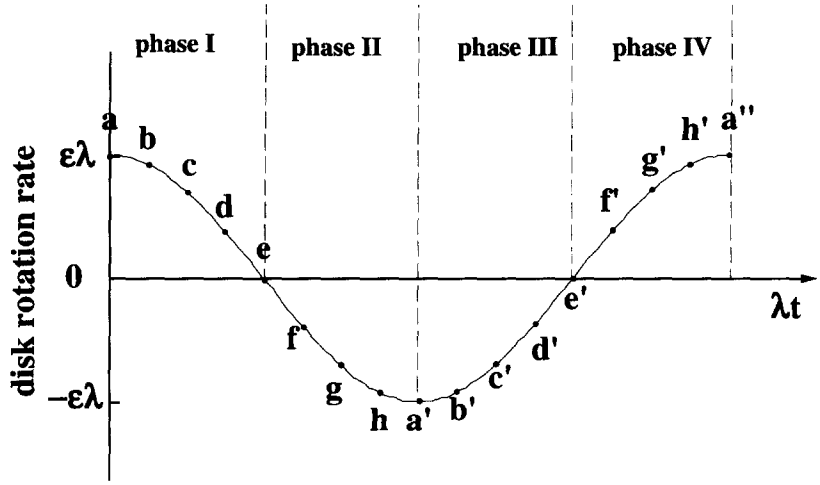

Fig. 8. Evolution of the angular velocity of the top disk.

crucial part in the discussion is the temporal behavior of Ψ_f relative to the steady streaming.

Sequential plots of Ψ_f and θ_f ($\equiv \theta - z/Ar - \theta_s$) the fluctuating part of temperature deviation, for the resonance case ($St_{re} \cong 2.6$) are illustrated in Fig. 9. Note that the temperature field θ_f displayed here represents the deviations relative to the original, conduction-dominant vertically-linear profile. It should be remembered that the full instantaneous flow field consists of these fluctuating parts and the more prominent steady flows portrayed in Fig. 2.

First, the flow evolution is scrutinized. At time τ_a, the full domain is occupied by a clockwise (CW) circulation cell, which was developed by the disk acceleration in the previous oscillation cycle. At time τ_b, a weak counterclockwise (CCW) circulation forms near the stationary bottom disk. As the rotation rate of the disk approaches zero (see frames c, d, e), the CCW grows from the bottom and fills most of the cylinder. In phases II, a reverse process takes place. In summary, in a half cycle, the CW and CCW circulating cells are developed and they disappear subsequently.

In an endeavour to identify heat transport under resonance conditions, the movements of the cold spots, relative to the steady temperature field, are traced. In Fig. 9(a), a cold spot, characterized by negative values of θ_f, is visible in the bottom region of the cylinder. This represents the vertical intrusion of cold disturbances (from the bottom cold disk) which were developed in the acceleration phase ($\tau = \tau_a$) of the previous cycle. These disturbances were transported by the general upwelling motions of the steady streaming. As is discernible in Figs 9(b) and (c), this cold disturbances travels upward in much of the interior region. Only in a zone close to the cylindrical sidewall, hot disturbances are seen. These represent the downwelling near the sidewall, carrying hot fluids which were in contact with the top hot disk. Around $\tau = \tau_d$ and $\tau = \tau_e$, the cold disturbances are broken into two parts. One forms the cold zone in the upper region, adjacent to the top disk; another is found in the sidewall area of the bottom region of the cylinder. The upper cold disturbance weakens and subsequently dies out. The bottom cold zone moves toward the axis and later moves upward as described earlier.

The above pictures provide a clue for the resonant convection. While the cold disturbance is in contact with the top hot disk, heat transfer takes place. This heated fluid travels downward at large radii due to the

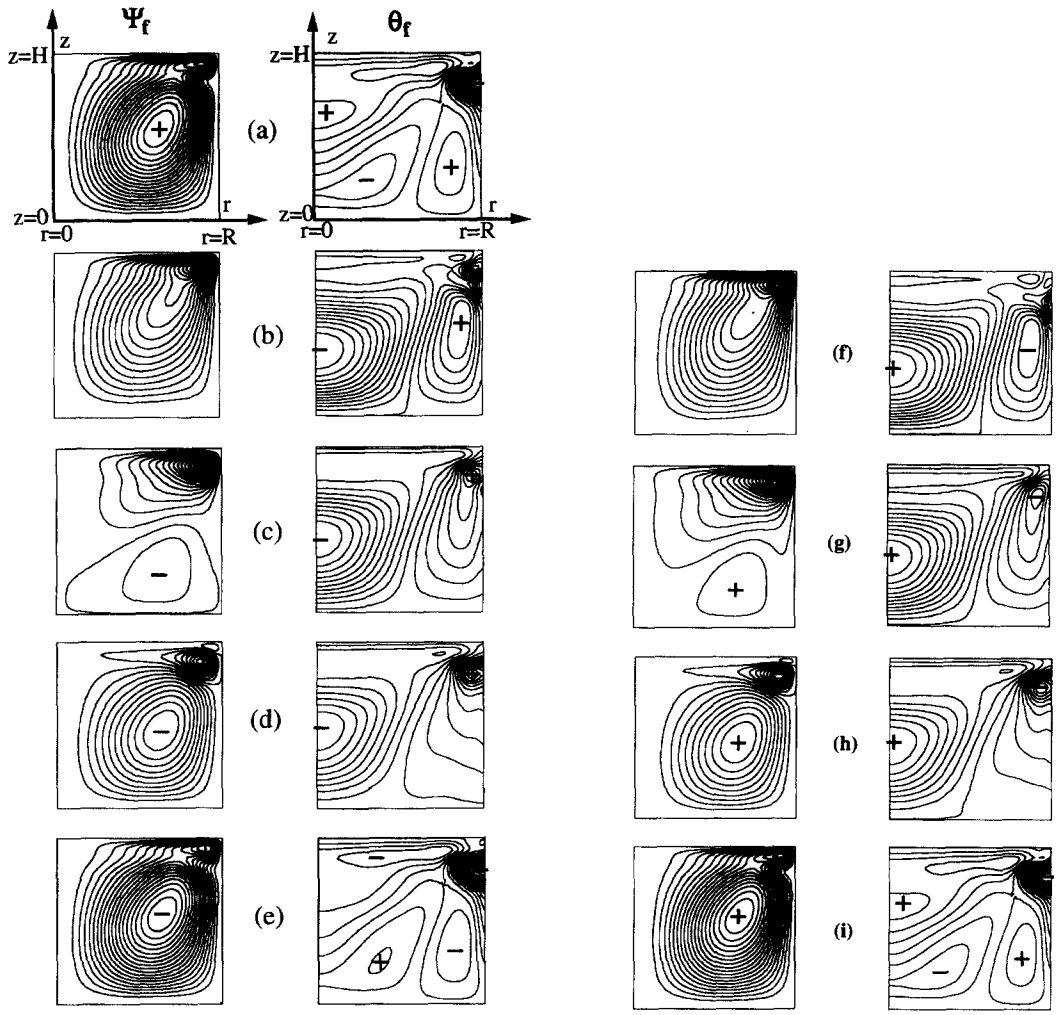

Fig. 9. Plots of meridional stream function Ψ_f for the fluctuating meridional flow (u_f, w_f), and fluctuating temperature θ_f, under resonance condition, i.e., $St_\lambda = St_{re} = 2.6$, $Re = 1000$, $\varepsilon = 2.5$. Times for the frames are (a) $\lambda t = 0$, (b) $\lambda t = \pi/8$, (c) $\lambda t = \pi/4$, (d) $\lambda t = 3\pi/8$, (e) $\lambda t = \pi/2$, (f) $\lambda t = 5\pi/8$, (g) $\lambda t = 3\pi/4$, (h) $\lambda t = 7\pi/8$, (i) $\lambda t = \pi$.

steady streaming, and when this hot fluid gets into contact with the bottom cold disk, heat is transferred from the fluid to the bottom disk. Therefore, the key assertion is that, in order to achieve maximum heat transfer, the two events, i.e., (1) the generation and disappearance of cold and hot spots; and (2) the development and diminishing of the CW and CCW circulations, are synchronized. When this is satisfied, resonance is materialized. The frequency of event (1) is characterized by the inertial–gravity oscillation, and event (2) is largely controlled by external excitation of frequency 2λ. As seen in Fig. 9, when 2λ and σ_{mn} are approximately equalized, flow and heat transfer take place in a broader region of the cylinder and the intensities of these are increased.

The qualitative pictures of temporal behaviour of Ψ_f and θ_f under off-resonance conditions are exemplified in Figs 10 and 11. In Fig. 10, $St_\lambda > St_{re}$, which can be interpreted as $\lambda < \lambda_{re}$ if N is unaltered. The external excitation is of low frequency. The period of external forcing is longer than the period of the occurrence and disappearance of hot and cold spots. This mismatch of the two times leads to a lower effective heat transfer rate. As seen, the patterns of fluctuating part of flow produce vertically-stacked circulation cells, which undercuts vigorous convective activities. This feature was emphasized in Kwak and Hyun (1996). In Fig. 11, a qualitatively opposite case is demonstrated. For a fixed N, $\lambda > \lambda_{re}$, reflecting the fact that the external excitation is of high frequency. The mismatch of the above-described two times is seen. The velocity patterns produce a horizontally-stacked structure, which lessens effective convective heat transport (see Kwak and Hyun, 1996).

In the related studies on natural-convection resonance in a cavity (Kwak and Hyun, 1996; Antohe and Lage, 1994), the time evolutions of the surface-averaged Nu values at the walls were plotted. Under resonance, the Nusselt numbers everywhere in the cavity show oscillations with varying amplitudes depend-

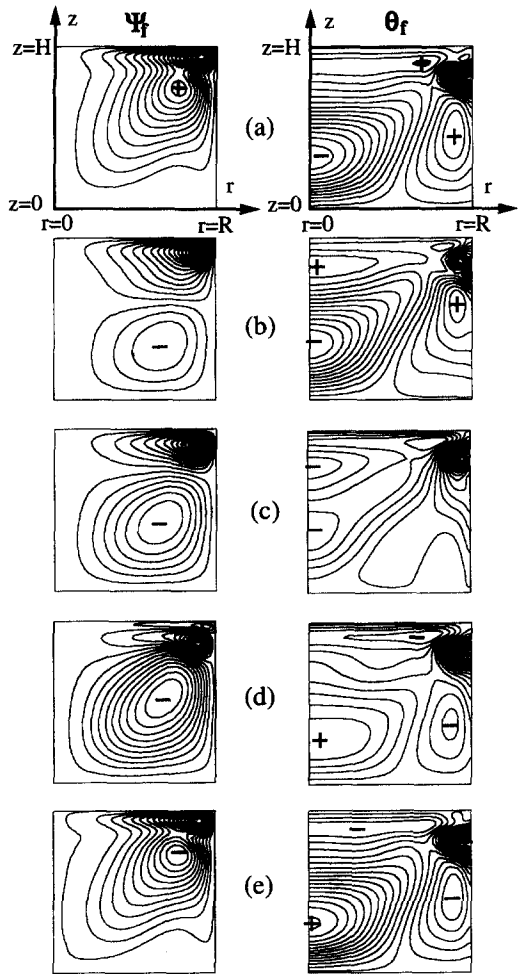

Fig. 10. Plots of meridional stream function Ψ_f for the fluctuating meridional flow (u_f, w_f), and fluctuating temperature θ_f, under off-resonance condition, i.e., $St_\lambda = 3.0$, $Re = 1000$, $\varepsilon = 2.5$. Times for the frames are (a) $\lambda t = 0$, (b) $\lambda t = \pi/8$, (c) $\lambda t = \pi/4$, (d) $\lambda t = 3\pi/8$, (e) $\lambda t = \pi/2$.

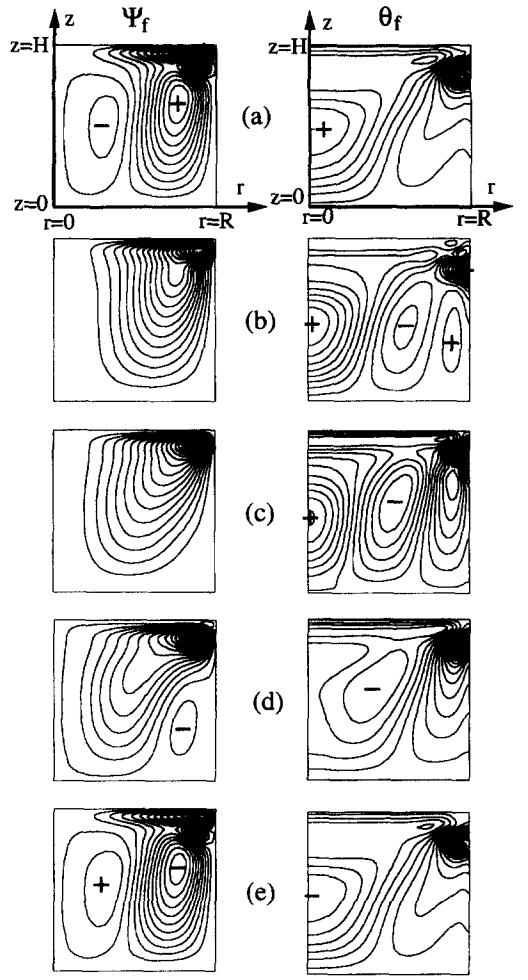

Fig. 11. Plots of meridional stream function Ψ_f for the fluctuating meridional flow (u_f, w_f), and fluctuating temperature θ_f, under off-resonance condition, i.e., $St_\lambda = 2.2$, $Re = 1000$, $\varepsilon = 2.5$. Times for the frames are (a) $\lambda t = 0$, (b) $\lambda t = \pi/8$, (c) $\lambda t = \pi/4$, (d) $\lambda t = 3\pi/8$, (e) $\lambda t = \pi/2$.

ing on the locations. Qualitatively similar pictures prevail in the present study. The changes in the time-evolutions with the forcing frequency were delineated explicitly in the preceding accounts (see Fig. 4 of Kwak and Hyun, 1996).

4. CONCLUSION

As the overall stratification increases, the steady meridional streaming is concentrated to a narrow region to the top disk. Inspection of the fluctuating parts of meridional velocity and of the Nusselt number leads to the identification of resonance conditions.

The frequencies σ_{mn} of the inertial–gravity oscillations, as obtained by inviscid analysis provide reasonably accurate descriptions of the system eigenfrequencies. For meridional flows, when excitation frequency 2λ is equal to σ_{mn}, resonance takes place. Substantial enhancements of $A(\Psi_f)$ and $A(Nu_f)$ are realized under resonance conditions, and this phenomenon is pronounced in the middle portion of the cylinder.

A scrutiny of the flow evolutions is supportive of the above assertion that flow and heat transport are augmented when the resonance condition is stratified.

Acknowledgements—Appreciation is extended to the referees whose constructive and helpful comments led to improvements in the revised manuscript.

REFERENCES

1. Aldredge, K. D., Axisymmetric inertial oscillations of fluid in a cylindrical cavity during spin-up from rest. *Geophys. Astrophys. Fluid Dynamics*, 1976, **8**, 279–301.
2. Alonso, C. V., Steady laminar flow in a stationary tank with a spinning bottom. *ASME Journal of Applied Mech.*, 1975, **42**, 771–776.
3. Antohe, B. V. and Lage, J. L., A dynamic thermal insulator : inducing resonance within a fluid saturated porous medium enclosure heated periodically from the side. *Int. J. Heat Mass Transfer*, 1994, **37**, 771–782.
4. Antohe, B. V. and Lage, J. L., Experimental inves-

tigation on pulsating horizontal heating of a water filled enclosure. *ASME J. Heat Transfer*, 1996, **118,** 889–896.
5. Antohe, B. V. and Lage, J. L., The Prandtl number effect on the optimum heating frequency of an enclosure filled with fluid or with a saturated porous medium. *Int. J. Heat Mass Transfer*, 1997, **40,** 1313–1323.
6. Benney, D. J., The flow induced by a disk oscillating in its own plane. *Journal of Fluid Mech.*, 1964, **18,** 385–391.
7. Bertela, M. and Gori, F., Laminar flow in a cylindrical container with a rotating cover. *ASME J. of Fluids Engineering*, 1982, **104,** 31–39.
8. Greenspan, H. P., *The Theory of Rotating Fluids*. Cambridge University Press, 1968.
9. Hyun, J. M., Flowlis, W. F. and Warn-Varnas, A., Numerical solutions for the spin-up of a stratified fluid. *Journal of Fluid Mech.*, 1982, **117,** 71–90.
10. Hyun, J. M., Leslie, F., Flowlis, W. F. and Warn-Varnas, A., Numerical solutions for spin-up from rest in a cylinder. *Journal of Fluid Mech.*, 1983, **127,** 263–281.
11. Hyun, J. M., Unsteady buoyant convection in an enclose. *Advances in Heat Transfer*, 1994, **24,** 227–320.
12. Iwatsu, R., Hyun, J. M. and Kuwahara, K., Convection in a differentially-heated square cavity with a torsionally-oscillating lid. *Int. J. Heat Mass Transfer*, 1992, **35,** 1069–1076.
13. Kreith, F., Doughman, E. and Kozlowski, H., Mass and heat transfer from an enclosed rotating disk with and without source flow. *ASME Journal of Heat Transfer*, 1963, **May,** 153–162.
14. Kwak, H. S. and Hyun, J. M., Natural convection in an enclosure having a vertical sidewall with time-varying temperature. *Journal of Fluid Mech.*, 1996, **329,** 65–88.
15. Lage, J. L. and Bejan, A., The resonance of natural convection in an enclosure heated periodically from the side. *Int. J. Heat Mass Transfer*, 1993, **36,** 2027–2038.
16. Lang, E., Sridhar, K. and Wilson, N. W., Computational study of disk driven rotating flow in a cylindrical encloser. *ASME Journal of Fluids Engineering*, 1994, **116,** 263–281.
17. Lehmkull, G. D. and Hudson, J. L., Flow and mass transfer near an enclosed rotating disk: experiment. *Chemical Engineering Science*, 1971, **26,** 1601–1613.
18. Lim, T. G. and Hyun, J. M., Flow driven by a torsionally-oscillating endwall disk. *ASME Journal of Fluids Engineering*, 1997, **119,** 115–121.
19. Pao, H.-P., A numerical computation of a confined rotating flow. *ASME Journal of Applied Mech.*, 1970, **37,** 480–487.
20. Rosenblat, S., Torsional oscillations of a plane in a viscous fluid. *Journal of Fluid Mech.*, 1959, **5,** 206–220.
21. Schlichting, H., *Boundary Layer Theory*. Pergamon, London, 1968.
22. Sparrow, E. M. and Gregg, J. L., Mass transfer, flow, and heat transfer about a rotating disk. *ASME Journal of Heat Transfer*, 1960, **82,** 294–302.
23. Warn-Varnas, A., Fowlis, W. W., Piacsek, S. and Lee, S. M., Numerical solutions and laser-Doppler measurements. *Journal of Fluid Mech.*, 1978, **85,** 609–639.